

# The Light Quark Connected Hadronic Vacuum Polarization Contribution to the muon anomaly via Sparsened Meson Fields

Vaishakhi Moningi,<sup>a,\*</sup> Christopher Aubin,<sup>b</sup> Thomas Blum,<sup>a</sup> Maarten Golterman,<sup>c,d</sup> Luchang Jin<sup>a</sup> and Santiago Peris<sup>d</sup>

<sup>a</sup>*Dept. of Physics, Univ. of Connecticut,  
Storrs, CT 06269, USA*

<sup>b</sup>*Dept. of Physics & Engineering Physics, Fordham Univ.,  
Bronx, NY 10458, USA*

<sup>c</sup>*Dept. of Physics and Astronomy, San Francisco State Univ.,  
San Francisco, CA 94132, USA*

<sup>d</sup>*Dept. of Physics and IFAE-BIST, Univ. Autònoma de Barcelona,  
E-08193 Bellaterra, Barcelona, Spain*

*E-mail: [vaishakhi.moningi@uconn.edu](mailto:vaishakhi.moningi@uconn.edu)*

We present an update on our determination of the light-quark connected contribution to the hadronic vacuum polarization (HVP) of the muon anomalous magnetic moment,  $a_\mu$ , on a finer lattice with 2+1+1 highly-improved staggered quark (HISQ) ensemble from the MILC collaboration with physical pion mass, 0.042 fm lattice spacing, and size  $144^3 \times 288$  sites. Within the low-mode averaging (LMA) framework, the HVP correlator is decomposed into low-low (LL), high-low (HL), low-high (LH) and high-high (HH) components. Since the LL part dominates the total statistical uncertainty but is also the most computationally expensive to evaluate, we implement a sparsening strategy to construct the meson fields efficiently. This approach significantly reduces the computational cost while preserving signal quality. By combining the sparsened LL contribution with HL, LH and HH components, we achieve an improved determination of the light-quark connected HVP contribution to  $a_\mu$ .

*The 42nd International Symposium on Lattice Field Theory (LATTICE2025)  
2-8 November 2025  
Tata Institute of Fundamental Research, Mumbai, India*

---

\*Speaker

## 1. Introduction

The anomalous magnetic moment of the muon is defined as  $a_\mu = (g - 2)/2$ , where  $g$  is the Landé  $g$ -factor, proportional to the muon's intrinsic magnetic moment. In Dirac's relativistic quantum theory  $g = 2$  exactly, but in the Standard Model (SM) of particle physics it gets tiny corrections from the electromagnetic, strong, and weak interactions. Currently it offers one of the most stringent tests of the SM because it has been measured and computed with high precision. The new experimental world average, dominated by the measurements at Fermi National Accelerator Laboratory (FNAL), is  $a_\mu = 1165920715(145) \times 10^{-12}$  (124 ppb). The measurements at FNAL have improved the precision on the world average by over a factor of 4 [1]. A commensurate theoretical effort is necessary to match the expected experimental precision.

## 2. Theoretical framework

The leading-order hadronic vacuum polarization contribution to the muon anomalous magnetic moment  $a_\mu$  is obtained via [2–4]

$$a_\mu^{\text{HVP}} = 2 \int_0^\infty dt w(t) C(t) \quad (1)$$

where the kernel  $w(t)$  comes from quantum electrodynamics (QED) [4, 5] and  $C(t)$  is the Euclidean time correlation function of two electromagnetic currents, summed over all quark flavors and averaged over spatial directions to project onto zero spatial momentum.

The aim of lattice calculations is to efficiently obtain  $C(t)$  with as much precision as possible. To do this we use the techniques of low-mode averaging (LMA) [6, 7] and all-mode averaging (AMA) [8]. Both methods rely on the spectral decomposition of the quark propagator in terms of the eigenvectors of the lattice Dirac operator. The quark propagator from source point  $y$  to sink point  $x$ ,  $S(x, y)$  mathematically is given by the inverse of the Dirac operator,

$$S(x, y) = D^{-1}(x, y) = \sum_{\lambda \leq \lambda_N} \frac{\langle x | \lambda \rangle \langle \lambda | y \rangle}{\lambda} + \sum_{\lambda > \lambda_N} \frac{\langle x | \lambda \rangle \langle \lambda | y \rangle}{\lambda} = S_L + S_H, \quad (2)$$

where the RHS shows the spectral decomposition divided into two pieces, one for the low modes up to  $\lambda_N$  and one for the rest, or high modes. Accordingly, we separate  $C(t)$  into four parts: low-low (LL), low-high (LH), high-low (HL), and high-high (HH),

$$C(t) = \frac{1}{3} \sum_{\vec{x}, \vec{y}, i} \text{Tr} \gamma_i S(x, y) \gamma_i S(y, x) = C_{LL} + C_{LH} + C_{HL} + C_{HH}. \quad (3)$$

In practice, once the low modes are determined,  $S_H$  is determined by computing the inverse of the deflated Dirac operator, using the conjugate gradient algorithm. So, not only do the low modes significantly enhance our statistics through LMA, but they also dramatically accelerate the computation of the high mode part.

### 3. Lattice details

The lattice computation presented here extends the simulations reported in Ref. [9]. In the present work, we extend the analysis by incorporating a new fine ensemble, 144c, on which we compute the two-point correlation functions that together reconstruct the full correlator of Eq. (3). The results from the remaining five ensembles are taken from our previous calculation. All calculations are performed using gauge-field configurations generated by the MILC Collaboration with 2+1+1 flavors of HISQ quarks <sup>1</sup>. On the 144c ensemble, we compute 8000 (4000) low modes of the full (preconditioned) Dirac operator, enabling improved control of the long-distance behavior of the correlator. The lattice spacings are set using using the  $w_0 = 0.17187(68)$  fm which is determined using the mass of  $\Omega^-$  baryon [11] and  $w_0/a$  are obtained from v1 of Ref. [12]

Label	$m_\pi$ (MeV)	$a$ (fm)	$N_S^3 \times N_T$	$N_{\text{low}}$	# configs (LL-HL-HH)
144c	134.5	0.04262	$144^3 \times 288$	4000	20-22-27

**Table 1:** Lattice simulation details. “ $N_{\text{low}}$ ” is the number of low-modes of the preconditioned Dirac operator. The number of configurations used for measurements in this study are given in the last column.

### 4. Motivation

Obtaining our target precision becomes increasingly demanding on larger physical volumes, particularly for the 144c ensemble. We implement the separation of  $C(t)$  as mentioned above in Eq. (3) in Ref. [13]. This decomposition avoids redundant Dirac solves that would otherwise arise when the HH and HL terms are computed together and the LL contribution must be subtracted separately. Using this framework, the HL contribution is evaluated by forming stochastic linear combinations of low-mode sources on each time slice, reducing the number of solves to  $N_T \times N_{\text{hits}}$ , where  $N_T$  is the number of time slices. Here,  $N_{\text{hits}}$  denotes the number of independent stochastic samples per time slice. For each hit, a new set of random numbers is combined with the low-mode eigenvectors to form a stochastic source, and multiple hits are averaged to reduce the stochastic error in the HL estimate. This yields an improvement of 27% in the long-distance region (2.4–3.2 fm) in 64c ensemble for 10 hits. On larger lattices like 144c, only a single stochastic hit for HL was feasible due to the high computational cost.

Nevertheless, the LL term remains both the most computationally expensive and the dominant source of statistical uncertainty in the long-distance tail in Fig. (2). This motivates us to further optimize the LL contribution, which is the focus of the present work.

### 5. Low-low contribution to $C(t)$

On the lattice the local electromagnetic current is not conserved, so we use the point-split conserved current

$$J^\mu(x) = -\frac{1}{2}\eta_\mu(x)(\bar{\chi}(x + \hat{\mu})U_\mu^\dagger(x)\chi(x) + \bar{\chi}(x)U_\mu(x)\chi(x + \hat{\mu})) \quad (4)$$

<sup>1</sup>Our 48II ensemble in Table 2 is a CalLat ensemble [10]

where  $U_\mu$  are the gauge links for gauge invariance,  $\chi(x)$  are the single spin component staggered fermion fields, and  $\eta(x)$  arise from the spin diagonalization of the fermion action. To efficiently isolate the low-mode contribution, it is convenient to introduce the meson field, defined in the eigenmode basis of the Dirac operator as  $(\Lambda_\mu(t))_{n,m} = \sum_{\vec{x}} \langle n|x \rangle U_\mu(x) \langle x + \mu|m \rangle (-1)^{(m+n)(x+m)}$ , where  $n, m$  label eigenmodes of the Dirac operator, and the phases have been absorbed into the link variables,  $U_\mu(x)\eta_\mu(x) \rightarrow U_\mu(x)$ . Expressed in terms of these meson fields, the low-low (LL) contribution to the correlator takes a compact form,

$$C_{LL} = \frac{1}{4} \sum_{m,n} \sum_{\vec{x}} \frac{1}{\lambda_m \lambda_n} [\Lambda_\mu^\dagger(x)_{mn} \Lambda_\nu^\dagger(y)_{nm} + \Lambda_\mu^\dagger(x)_{mn} \Lambda_\nu(y)_{nm} + \Lambda_\mu(x)_{mn} \Lambda_\nu^\dagger(y)_{nm} + \Lambda_\mu(x)_{mn} \Lambda_\nu(y)_{nm}], \quad (5)$$

where  $\lambda_n$  is shorthand for  $i\lambda_n + m$ .

## 5.1 Sparsening of Meson Fields

The cost of the meson field scales linearly in the size of the lattice and quadratically with the number of eigenvectors which is prohibitive when both are large as in the case of the  $144^3 \times 288$  lattice. To significantly speedup the calculation, we “sparsen” the eigenvectors by omitting some number of sites in a regular pattern, *i.e.*, omit  $s$  consecutive points, evenly spaced, in each direction. This is increasingly effective as  $a \rightarrow 0$  since nearby points will be more and more correlated, and including them in the average does not meaningfully improve the statistical error. Sparsening also drastically reduces the memory footprint which is important if later we decide to increase the number of eigenvectors.

To ensure we preserve the spin-taste structure of the staggered fermion currents, the sparsening is done by choosing the location for a *hypercube* randomly on a given time-slice, and then we omit every  $s$  number of hypercubes in each spatial direction. In other words we always keep all points in a kept hypercube. By randomly choosing the initial hypercube on a time-slice we are guaranteed to project onto zero spatial momentum in the average. Sparsening by a factor  $(s, t)$  reduces the size of eigenvectors required to compute our meson fields from  $N_S^3 \times N_T$  to  $(N_S/s)^3 \times (N_T/t)$ . This reduction lead to a substantial increase in computational speed for the meson fields. Importantly, sparsening is limited to a factor of 4 in each dimension to avoid a noticeable increase in noise.

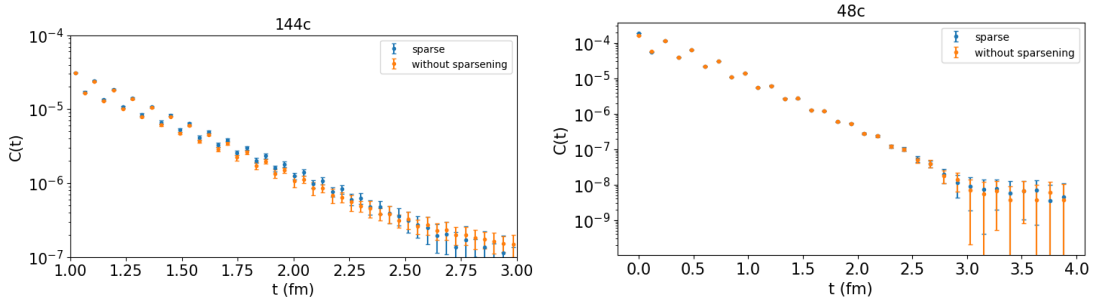


**Figure 1:** Left: Sparsening of factor  $(s=4, t=1)$  on 6 different configurations on 144c ensemble. Right: Sparsening of factor  $(s=2, t=1)$  on the same 24 configurations on 48I ensemble

## 6. Results

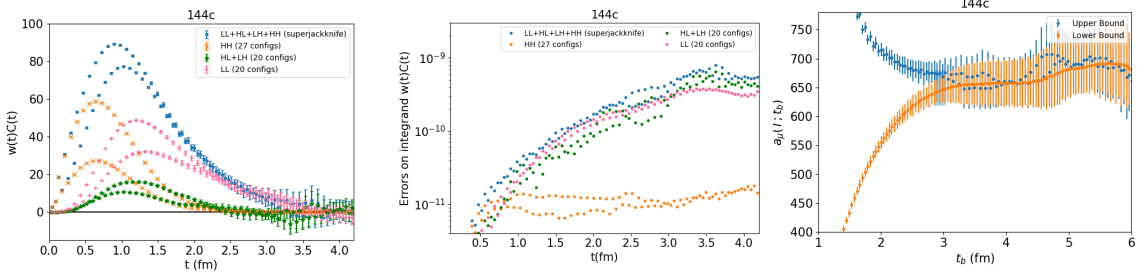


**Figure 2:** Left: Summand in  $w(t)C(t)$  Eq. (3). Middle: Quantitative breakdown of the statistical error in terms of LL, HH, HL on the summand. Right:  $(a_\mu(T; t_b))$  using the bounding method, as a function of the switch-point  $t_b$ .

Lattice simulations on the 144c ensemble yield the correlator  $C(t)$  defined in Eq. (1). We then define the trapezoid integration on the lattice,

$$a_\mu(t) \xrightarrow{a \rightarrow 0} 2 \int_0^{t/2} dt' w(t') C(t') = 2a \sum_{n=0}^{\lfloor t/2a \rfloor - 1} w(na) C(na) + aw(\lfloor t/2a \rfloor a) C(\lfloor t/2a \rfloor a), \quad (6)$$

where the maximum value of  $t/a$  is  $N_T$ . The bounding method [14, 15] on the correlation function is also applied in the time integration. We define the upper and lower bound of the two-point correlation function as, for  $t \leq T$ ,  $C_b(t) = C(t)$ , and for  $t > T$ ,  $C_b(t) = 0$  (lower bound) and  $C_b(t) = C(T) e^{-E_0(t-T)}$  (upper bound) where  $E_0 = 2\sqrt{m_\pi^2 + (2\pi/L)^2}$ .  $E_0$  denotes the (non-interacting) two-pion energy state. By using this method, we do not have to sum over the whole range of time slices to compute  $a_\mu^{\text{HVP}}$ , which contain the noisy long-distance tail. Instead, an estimate can be got from the overlap between the two bounds in large  $T$ . The statistical errors on the averages are computed using the jackknife method.

We incorporate finite-volume (FV), taste-breaking (TB) and pion-mass retuning effects into our lattice determination, see Table 2. The analysis proceeds in stages. These corrections are computed in NLO and NNLO SChPT, as well as in the chiral vector model (ChVM) developed specifically for the case of staggered fermions in Ref. [16] and applied further in Refs. [9, 17, 18]. For each ensemble, we first apply the NNLO finite-volume correction, the corresponding taste-breaking correction, and the adjustment accounting for pion-mass mistuning. The corrected results are then extrapolated to the continuum limit using an  $a^2$  ansatz based on six ensembles (five different lattice spacings). Our extrapolated values from these fits are as follows:

$$\text{NNLO} : a_\mu^{\text{HVP}, \text{lqc}} = (656.5 \pm 9.2) \times 10^{-10} \text{ without TB}, \quad (664.4 \pm 9.2) \times 10^{-10} \text{ with TB} \quad (7)$$

$$\text{ChVM} : a_\mu^{\text{HVP}, \text{lqc}} = (647.5 \pm 9.2) \times 10^{-10} \text{ without TB}, \quad (657.3 \pm 9.2) \times 10^{-10} \text{ with TB} \quad (8)$$

We take the average of these fits with and without taste breaking in their respective scheme as our best value

$$\text{NNLO} : a_\mu^{\text{HVP}, \text{lqc}} = (660.5 \pm 9.2 \pm 4.0 \pm 1.9 \pm 0.3) \times 10^{-10} = 661(10) \times 10^{-10} \quad (9)$$

$$\text{ChVM} : a_\mu^{\text{HVP}, \text{lqc}} = (652.4 \pm 9.2 \pm 4.9) \times 10^{-10} = 652(10) \times 10^{-10} \quad (10)$$

Ensemble	HVP,lqc $a_\mu$	w1,lqc $a_\mu$	w2,lqc $a_\mu$
144c	658.4 (15.3) (4.7)	207.36 (49) (34)	98.4 (1.9) (1.0)
96c	609.3 (13.0) (4.4)	206.14 (38) (34)	95.2 (2.4) (1.1)
64c	599.8 (9.3) (4.3)	205.27(26)( 37)	88.9 (1.3) (1.1)
48I	552.3(8.6) (4.0)	201.96 (53) (42)	78.2 (1.4) (1.0)
48II	522.7 (8.0) (3.8)	199.78 (42) (44)	72.5 (1.2) (1.0)
32c	505.3 (6.9) (3.7)	200.64 (68) (45)	71.3 (1.0) (1.0)

**Table 2:** Lattice results for  $a_\mu^{\text{HVP,lqc}}$ , the 0.4–1.0 fm window  $a_\mu^{\text{w1,lqc}}$  and the 1.5–1.9 fm window  $a_\mu^{\text{w2,lqc}}$ . The first error is statistical, the second error from scale setting.

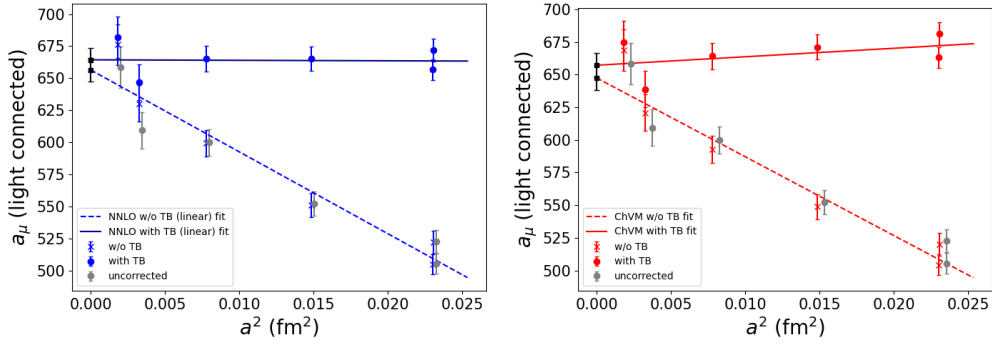


**Figure 3:** Left: SchPT NNLO fits – linear, blue (dashed=no TB, solid=TB). Right: ChVM fits – linear, red (dashed=no TB, solid=TB). Data points match fit colors; continuum limits in black. Gray points show uncorrected values from Table 2.

For all fits, we have assumed the statistical errors to be uncorrelated, since the data are obtained on different ensembles and the scale-setting error is folded into the fit error, as we took the scale-setting errors of Table 2 into account in our fits, assuming them to be 100% correlated. The four errors in Eq. (9) are statistical error from the fit, half the difference between the two fits with and without TB, and the errors on the NNLO FV and retuning corrections closest to the average (144c ensemble). The error in the second equality in Eqs. (9) and (10) is obtained by adding these errors in quadrature.

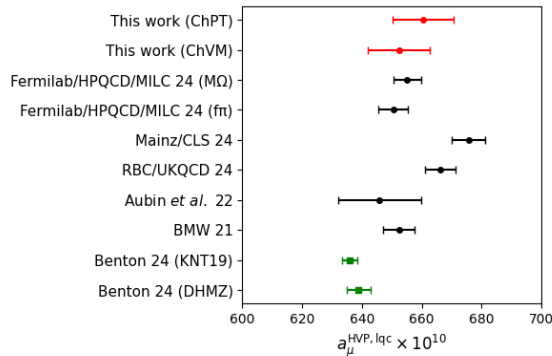


**Figure 4:** Comparison of our lattice determinations for  $a_\mu^{\text{HVP,lqc}}$  (red circles) with other lattice results (black circles) and data-driven results (green squares)

In Fig. (4) we compare our result for  $a_\mu^{\text{HVP,lqc}}$  with previous lattice-QCD calculations as well as the data-driven evaluations. With our updated results in Eq. 9 (resp. (10)), we find significances in the differences of  $0.47\sigma$  ( $0.25\sigma$ ) with Fermilab/HPQCD/MILC 24 using  $M_\Omega$  and  $0.88\sigma$  ( $0.16\sigma$ ) using  $f_\pi$  [19],  $0.50\sigma$  ( $1.19\sigma$ ) with RBC/UKQCD 24 [20],  $1.31\sigma$  ( $1.98\sigma$ ) with Mainz/CLS 24 [21],  $0.85\sigma$  ( $0.37\sigma$ ) with Aubin 22 [9] and  $0.70\sigma$  ( $0.0\sigma$ ) with BMW 21 [18]. Finally, we find that our result differs from the data-driven evaluation such as Benton 24 by  $2.35\sigma$  ( $1.55\sigma$ ) using KNT and  $1.97\sigma$  ( $1.21\sigma$ ) using DHMZ [22]. This tension clearly indicates the need for more precise calculation.

## 6.1 Window Quantities

We further investigate  $a_\mu$  for the intermediate window [15] as it is used to make more precise comparisons with others since it focuses on medium-time-distance region where the results are more precise.

$$a_\mu = 2 \sum_{t=0}^{T/2} C(t)w(t) (\Theta(t, t_0, \Delta) - \Theta(t, t_1, \Delta)), \quad \text{with } \Theta(t, t', \Delta) = \frac{1}{2} \left( 1 + \tanh \frac{t - t'}{\Delta} \right) \quad (11)$$

### 6.1.1 Window 0.4-1.0 fm

We show  $a_\mu^{\text{W1,lqc}}$  as a function of  $a^2$ . Our extrapolated values from these fits are as follows:

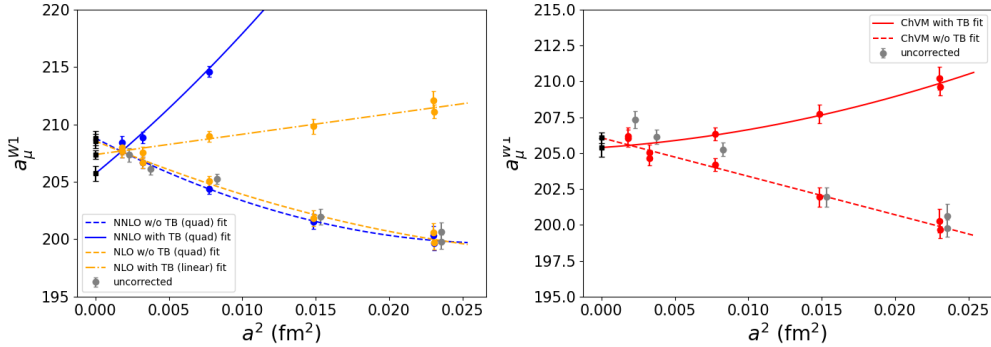


**Figure 5:** Left: SCHPT fits - NNLO quadratic, blue (dashed = no TB, solid = with TB). NLO yellow: quadratic (dotted = no TB) and linear (dot-dashed = with TB). Right: ChVM quadratic, red (dashed = no TB, solid = with TB). Continuum limits in black. Gray points show uncorrected values from Table 2.

$$\text{ChVM} : a_\mu^{\text{W1,lqc}} = (206.07 \pm 0.38) \times 10^{-10} \text{ without TB}, (205.39 \pm 0.64) \times 10^{-10} \text{ with TB} \quad (12)$$

Applying chiral perturbation theory (ChPT) to estimate finite-volume and taste-breaking corrections for the intermediate window quantity  $a_\mu^{\text{W1}}(0.4, 1.0; 0.15)$  (with values of the arguments in fm) is not fully justified, since this window is restricted to distances below 1 fm and is therefore not dominated by purely long-distance physics where ChPT is expected to be reliable. This motivates the use of phenomenological models such as ChVM. However, while such models can describe the data within a limited range, they cannot provide controlled extrapolations beyond it. Consequently, for this window, continuum and infinite-volume limits cannot be obtained from lattice data alone

without introducing model dependence, as no fully reliable EFT description is available in this regime.

For this reason, we also consider a longer-distance window,  $a_\mu^{\text{W}2}(1.5, 1.9; 0.15)$  (with values of the arguments in fm), which is more firmly in the long-distance regime and therefore better suited for treatment within ChPT.

### 6.1.2 Window 1.5-1.9 fm

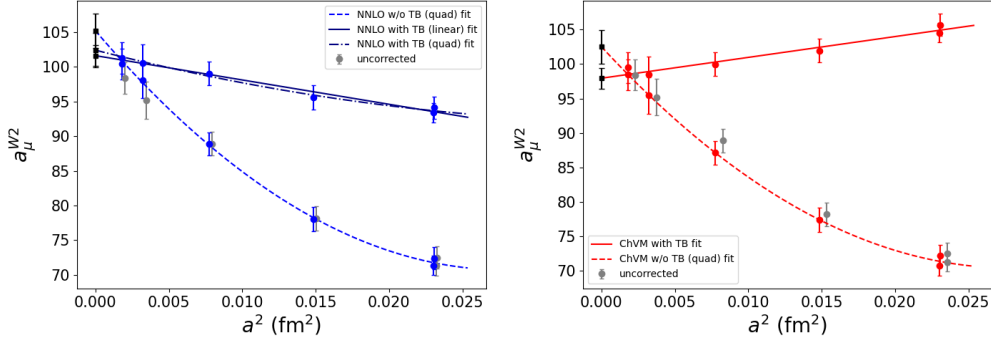


**Figure 6:** Left: SChPT NNLO fits - quadratic, blue (dashed=no TB, dotted-dashed=TB) and linear, blue (solid=TB). Right: ChVM fits - quadratic, red (dashed=no TB, solid=TB). Data points match fit colors; continuum limits in black. Gray points show uncorrected values from Table 2.

$$\text{NNLO} : a_\mu^{\text{W}2, \text{lqc}} = (105.2 \pm 2.5) \times 10^{-10} \text{ without TB, } (101.6 \pm 1.5) \times 10^{-10} \text{ with TB linear} \quad (13)$$

$$\text{ChVM} : a_\mu^{\text{W}2, \text{lqc}} = (102.5 \pm 2.5) \times 10^{-10} \text{ without TB, } (97.9 \pm 1.5) \times 10^{-10} \text{ with TB} \quad (14)$$

## 7. Conclusion

In our earlier analysis, based on ensembles up to 96c, we obtained  $a_\mu^{\text{HVP, lqc}} = 646(14) \times 10^{-10}$  using NNLO SChPT and  $638(14) \times 10^{-10}$  using ChVM. With the addition of the 144c ensemble, these values become  $661(10) \times 10^{-10}$  and  $652(10) \times 10^{-10}$ , respectively, corresponding to a reduction in the total uncertainty by a factor of 1.4.

Compared to our previous work, the present calculation achieves a quantitative improvement in precision primarily through improved control of the light-quark connected contribution, driven by the 144c ensemble. Although our total uncertainty remains larger than the most precise determinations, further reduction is expected by increasing statistics on the fine lattices; in particular, we plan to double up the statistics to reduce the error and achieve our sub-present goal.

In Fig. (2 (middle)), we observe that the HL contribution, while subdominant in the total integral, develops a rapidly growing uncertainty at large Euclidean times. One straightforward way to control this behavior is to increase the number of hits per configuration, though this becomes computationally expensive on 144c. An alternative and potentially more efficient strategy is to develop a multi-grid [23] or AMA-inspired machine learning framework [24] that predicts the long-distance HL contribution at significantly reduced cost. Such an approach could provide improved statistical precision in the tail region without a proportional increase in computational resources.

a (fm)	$a_{\mu}^{\text{HVP,lqc}} \times 10^{-10}$	$a_{\mu}^{\text{W1,lqc}} \times 10^{-10}$	$a_{\mu}^{\text{W2,lqc}} \times 10^{-10}$
0.04262(17)	658(15)(5)[15]	207.3(5)(3)[6]	98.4(1.9)(1.0)[2.1]
0 (NNLO ChPT)	661(9)(4)[10]		103.4(2.5)(1.8)[3.1]
0 (ChVM)	652(9)(5)[10]	205.7(6)(3)[7]	100.2(2.5)(2.3)[3.3]

**Table 3:** HVP contributions to the muon anomaly using NNLO SChPT and ChVM. First row errors: (statistical)(scale)[tot]; Second+Third row errors: (fit error)(sys)[tot]. Systematic error is taken as half the difference between the continuum extrapolated results with and without TB.

## Acknowledgments

We gratefully acknowledge support by the U.S. Department of Energy, Office of Science, Office of High Energy Physics, under Awards DE-SC0013682 (MG), DE-SC0021147, DE-SC0010339 and DE-SC0026314 (LJ) and DE-SC0010339 (TB,VM). SP is supported by the Spanish Ministerio de Ciencia e Innovacion, grants PID2020-112965GB-I00 and PID2023-146142NB-I00, and by the Departament de Recerca i Universitats from Generalitat de Catalunya to the Grup de Recerca 00649 (Codi: 2021 SGR 00649). IFAE is partially funded by the CERCA program of the Generalitat de Catalunya. The authors acknowledge the [Texas Advanced Computing Center \(TACC\)](#) at The University of Texas at Austin for providing computational resources on Frontera, Stampede 2, and Stampede 3 that have contributed to the research results reported in this proceedings.

## References

- [1] S. Donati et al., *Measurement of the positive muon anomalous magnetic moment to 127 ppb*, *Phys. Rev. Lett.* **135** (2025) 101802.
- [2] B.e. Lautrup, A. Peterman and E. de Rafael, *Recent developments in the comparison between theory and experiments in quantum electrodynamics*, *Phys. Rept.* **3** (1972) 193.
- [3] E. de Rafael, *Hadronic contributions to the muon  $g-2$  and low-energy QCD*, *Phys. Lett.* **B322** (1994) 239 [[hep-ph/9311316](#)].
- [4] T. Blum, *Lattice calculation of the lowest order hadronic contribution to the muon anomalous magnetic moment*, *Phys.Rev.Lett.* **91** (2003) 052001 [[/0212018](#)].
- [5] D. Bernecker and H.B. Meyer, *Vector Correlators in Lattice QCD: Methods and applications*, *Eur.Phys.J.* **A47** (2011) 148 [[1107.4388](#)].
- [6] L. Giusti, P. Hernandez, M. Laine, P. Weisz and H. Wittig, *Low-energy couplings of QCD from current correlators near the chiral limit*, *JHEP* **04** (2004) 013 [[/0402002](#)].
- [7] T.A. DeGrand and S. Schaefer, *Improving meson two point functions in lattice QCD*, *Comput. Phys. Commun.* **159** (2004) 185 [[/0401011](#)].
- [8] T. Blum, A. Denig, I. Logashenko, E. de Rafael, B. Lee Roberts et al., *The Muon ( $g-2$ ) Theory Value: Present and Future*, [1311.2198](#).
- [9] C. Aubin, T. Blum, M. Golterman and S. Peris, *Muon anomalous magnetic moment with staggered fermions: Is the lattice spacing small enough?*, *Phys. Rev. D* **106** (2022) 054503 [[2204.12256](#)].

- [10] Z.B. Hall, D.A. Pefkou, A.S. Meyer, T.R. Richardson, R.A. Briceño, M.A. Clark et al., *Signs of non-monotonic finite-volume corrections to  $g_a$* , [2503.09891](#).
- [11] A. Bazavov, C.W. Bernard, D.A. Clarke, C. DeTar, A.X. El-Khadra, E. Gámiz et al., *High-precision scale setting with the omega-baryon mass and gradient flow*, *Phys. Rev. D* (2026) .
- [12] FERMILAB LATTICE, HPQCD, AND MILC COLLABORATIONS collaboration, *Hadronic vacuum polarization for the muon  $g - 2$  from lattice qcd: Complete short and intermediate windows*, [2411.09656](#).
- [13] V. Moningi, C. Aubin, T. Blum, M. Golterman, L. Jin and S. Peris, *Progress on computing the hadronic vacuum polarization contribution to the muon anomalous magnetic moment with staggered fermions*, *PoS LATTICE2024* (2025) 247.
- [14] BUDAPEST-MARSEILLE-WUPPERTAL collaboration, *Hadronic vacuum polarization contribution to the anomalous magnetic moments of leptons from first principles*, *Phys. Rev. Lett.* **121** (2018) 022002 [[1711.04980](#)].
- [15] RBC, UKQCD collaboration, *Calculation of the hadronic vacuum polarization contribution to the muon anomalous magnetic moment*, *Phys. Rev. Lett.* **121** (2018) 022003 [[1801.07224](#)].
- [16] B. Chakraborty, C. Davies, P. De Oliveira, J. Koponen, G. Lepage, H. Collaboration) et al., *Hadronic vacuum polarization contribution to a  $\mu$  from full lattice qcd*, *Physical Review D* **96** (2017) 034516.
- [17] C.T. Davies, C. DeTar, A. El-Khadra, E. Gamiz, S. Gottlieb, D. Hatton et al., *Hadronic-vacuum-polarization contribution to the muon's anomalous magnetic moment from four-flavor lattice qcd*, *Phys. Rev. D* **101** (2020) 034512.
- [18] S. Borsanyi, Z. Fodor, J. Guenther, C. Hoelbling, S. Katz, L. Lellouch et al., *Leading hadronic contribution to the muon magnetic moment from lattice qcd*, *Nature* **593** (2021) 51.
- [19] FERMILAB LATTICE, HPQCD, AND MILC COLLABORATIONS collaboration, *Hadronic vacuum polarization for the muon  $g - 2$  from lattice qcd: Long-distance and full light-quark connected contribution*, *Phys. Rev. Lett.* **135** (2025) 011901.
- [20] T. Blum, P. Boyle, M. Bruno, B. Chakraborty, F. Erben, V. Gülpers et al., *Long-distance window of the hadronic vacuum polarization for the muon  $g-2$* , *Physical Review Letters* **134** (2025) 201901.
- [21] D. Djukanovic, G. von Hippel, S. Kuberski, H.B. Meyer, N. Miller, K. Ottnad et al., *The hadronic vacuum polarization contribution to the muon  $g-2$  at long distances*, *Journal of High Energy Physics* **2025** (2025) 1.
- [22] G. Benton, D. Boito, M. Golterman, A. Keshavarzi, K. Maltman and S. Peris, *Data-driven results for light-quark connected and strange-plus-disconnected hadronic  $g-2$  short-and long-distance windows*, *Phys. Rev. D* **111** (2025) 034018.
- [23] R.C. Brower, E. Weinberg, M.A. Clark and A. Strelchenko, *Multigrid algorithm for staggered lattice fermions*, *Phys. Rev. D* **97** (2018) 114513.
- [24] T. Blum, A. Conigli, L. Geyer, S. Kuberski, A. Segner and H. Wittig, *Machine-learning techniques as noise reduction strategies in lattice calculations of the muon  $g - 2$* , in *41st International Symposium on Lattice Field Theory*, 2, 2025 [[2502.10237](#)].